The Selectivity-Activity Trade-off: Navigating Thermal Dynamics in CO_2 Hydrogenation to Ethanol over Supported Catalysts

Student

Rayan Alarishi | rayan.Alarishi@kaust.edu.sa

Supervisor

Professor Kuo-Wei Huang | kuowei.huang@kaust.edu.sa

Research Mentor

Dr. Rajesh Belgamwar | rajesh.belgamwar@kaust.edu.sa

Dr. Indranil Dutta | indranil.dutta@kaust.edu.sa

Abstract

The anthropogenic rise in atmospheric CO_2 necessitates scalable carbon dioxide utilization (CDU) strategies, with direct conversion to ethanol presenting a highly attractive pathway due to its utility as an energy-dense fuel and chemical feedstock. However, this thermo-catalytic process is fundamentally limited by the kinetic difficulty of C–C coupling and the thermodynamic dominance of competing C_1 pathways, such as methanation. In this study, we systematically synthesized and evaluated supported Cu-, Fe-, and Ir-based catalysts under high-pressure continuous-flow conditions (50 bar, H_2:CO_2 = 3:1) across a thermal gradient of 200–260 °C to navigate the inherent selectivity-activity trade-off. While highly dispersed Fe-Cu on crystalline CeO_2 and TiO_2 proved inactive due to a lack of contiguous dual-site domains, precision catalyst architectures successfully drove C_2 oxygenate formation. A 0.2 wt% $Ir_1/MgO–In_2O_3$ single-atom catalyst demonstrated remarkable low-temperature performance, achieving an exceptional ethanol selectivity of 27.5% at 200 °C by structurally isolating active centers to suppress extended-metal chain growth. Conversely, an in situ co-precipitated K-promoted mixed-oxide system (K-FexOx/ZnO/ZrO_2) leveraged adjacent, small-crystallite Fe_3O_4 and Fe_2O_3 domains to maximize overall throughput, yielding the highest absolute ethanol productivity of 22 μmol g^{-1} h^{-1} (at 4.3% CO_2 conversion) at an elevated temperature of 260 °C. These findings elucidate the complex mechanistic dichotomy of CO_2 hydrogenation, highlighting the critical role of rational phase engineering. This approach ranges from single-atom site isolation to synergistic mixed-oxide interfaces in stabilizing fragile C_2 oxygenate pathways and overcoming formidable thermodynamic barriers.

Contents

Contents *2*

1 Introduction *3*

2 Related Work *4*

3 Methodology *4*

3.1 Method details 5

3.2 Evaluation Procedure 5

4 Results and Discussion *6*

5 Limitations and Future Work *9*

6 Conclusion *9*

7 Acknowledgement *9*

References *10*

1 Introduction

The growing atmospheric carbon dioxide (CO_2) concentration exceeded 427 ppm in 2026 from 280 ppm before the industrial revolution because of anthropogenic activities and has become one of the most pressing issues associated with climate change.[1] The relentless trajectory of global fossil CO_2 emissions underscores the absolute urgency of this crisis. As illustrated in the historical and projected data Figure 1, emissions have persistently climbed over the past three decades. Between 2015 and 2024, emissions grew at a rate of +0.8% per year, and projections by the Global Carbon Project for 2025 indicate that global fossil CO_2 emissions will reach an unprecedented 38.1 Gt CO_2, representing a further 1.1% increase [2]. According to the IEA, CO_2 emissions reached a new record high of nearly 38.4 Gt in 2025.[3]

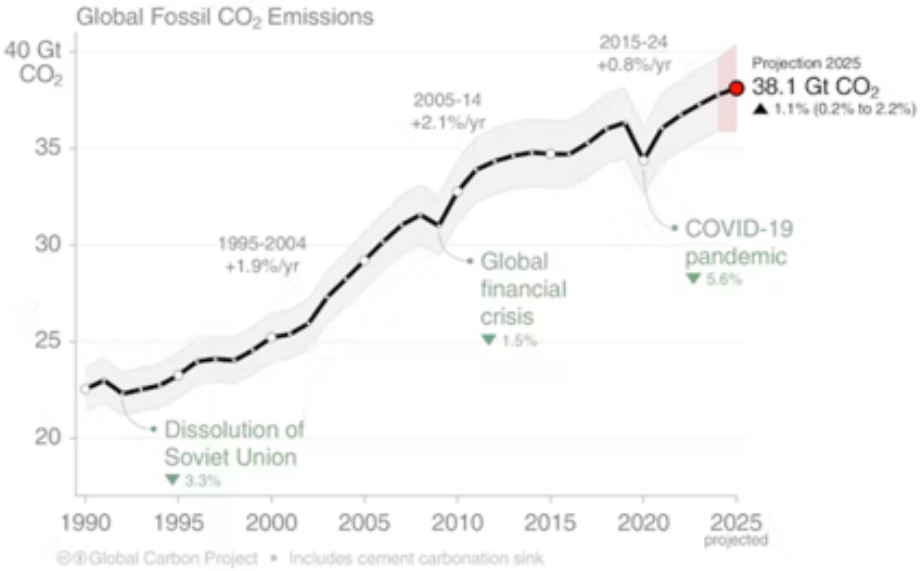


Figure 1. Recent global CO_2 emissions/temperature trend data.[3]

To meet the Paris Agreement objectives to keep global warming below 2 °C, carbon capture and utilization (CCU) and/or reduction of CO_2 emission of at least 30 gigatons of CO_2 ($GtCO_2$)/yr is needed.[1,4] To achieve a meaningful impact on both the economy and the environment, carbon dioxide utilization (CDU) must be conducted for profitable industrial applications in addition to net zero CO_2 emissions.[5,6] The importance of CDU in carbon management has long been recognized, and CO_2 is projected to play an essential role as the future C_1 raw material in the post-fossil fuels era.[7] However, at the present time, even if the carbon footprint of the energy consumption for CDU, with carbon in the most thermodynamically stable oxidation state of +4, is not considered, the scale of its impact is limited.[5]

The current CO_2 market potential for industrial use can reach merely 0.3–0.8 $GtCO_2$/yr in the best-case scenario, with the largest consumer of exhaust CO_2 emission being the fertilizer industry (~0.12–0.14 $GtCO_2$/yr used for urea manufacturing) followed by the oil sector (~0.07–0.08 $GtCO_2$/yr consumed for enhanced oil and/or gas recovery).[8] Alden and co-workers have also recently predicted CDU potential for CO_2 into chemicals to be around 0.3–0.6 $GtCO_2$/yr in 2050, and rationalized that CO_2-to-fuel has the highest estimated potential for CDU in the range of 1–4.2 $GtCO_2$/yr.[6]

Within this idea, the direct thermo-catalytic conversion of CO_2 to ethanol (Equation 1) is highly advantageous.

$$2CO_2 + 6H_2 \rightarrow C_2H_5OH + 3H_2O \quad \text{..... Equation 1}$$

Ethanol features a high liquid-phase energy density of 21 MJ L^{-1}. Furthermore, it serves as a valuable renewable fuel, a gasoline additive, and a versatile chemical feedstock.[10] This project aims to synthesize, characterize, and evaluate Cu-, Fe-, and Ir-based catalysts for CO_2 hydrogenation, seeking to suppress competing C_1 pathways and promote C–C coupling by navigating thermal dynamics between 200–260 °C.

2 Related Work

The direct conversion of CO_2 to ethanol is highly desirable for efficient carbon utilization, yet it remains one of the most catalytically challenging transformations due to the necessity of coupling two C_1 intermediates into a single C_2 product.[9] Current research highlights several fundamental kinetic and thermodynamic hurdles, which are addressed through advanced catalyst design: Competing C_1 Pathways and the Tandem Mechanism.[10]

Thermo-catalytic CO_2 hydrogenation typically proceeds via a complex tandem reaction network. Initially, CO_2 is reduced to CO via the endothermic reverse water-gas shift (RWGS) reaction.[11] The generated CO* then undergoes hydrogenation and coupling via Fischer-Tropsch (FT)-type mechanisms or formate-mediated CO insertion pathways. However, this network is severely plagued by competing C_1 pathways, most notably CO methanation, which acts as a thermodynamic sink and drastically limits ethanol selectivity.[10]

Iron-based catalysts are widely studied because they inherently possess the active sites required for both RWGS (typically via Fe_3O_4 phases) and subsequent C–C coupling[12]. Despite their high activity, traditional Fe-based catalysts suffer from poor product specificity. The chain growth mechanism adheres to the Anderson-Schulz-Flory (ASF) distribution, which inherently yields a broad, non-selective spectrum of C_1–C_n hydrocarbons and oxygenates [13]. To circumvent ASF limitations and suppress methanation, recent literature emphasizes the integration of alkali promoters (e.g., Potassium) and mixed-metal systems to tune the basicity and maintain a high density of oxygen vacancies on supports like ZnO/ZrO_2 [11,12].

This project builds upon these mechanistic foundations by systematically screening supported Cu-, Fe-, and Ir-based catalysts. By investigating the delicate interplay between promoter effects, mixed-oxide support architectures (e.g., CeO_2, TiO_2, In_2O_3), and thermal dynamics, this work aims to resolve current structure-function uncertainties and optimize the selectivity-activity trade-off.

3 Methodology

3.1 Method details

Preparation of 0.2 wt% $Ir_1/MgO–In_2O_3$ Single-Atom Catalyst

The mixed-oxide support was synthesized via a co-precipitation method. $In(NO_3)_3{\cdot}4.5H_2O$ (1.91 g) and $Mg(NO_3)_2{\cdot}6H_2O$ (0.64 g) were dissolved in a mixture of deionized water (10 mL) and ethanol

(25 mL). A precipitating agent comprising 25 wt% aqueous ammonia (6 mL) and anhydrous ethanol (20 mL) was added dropwise under vigorous stirring. The suspension was aged at 80 °C for 4 h, collected by centrifugation, washed thoroughly with deionized water, dried at 80 °C overnight, and calcined in static air at 500 °C for 3 h to yield the $MgO–In_2O_3$ support. The 0.2 wt% Ir single-atom catalyst was subsequently prepared by wet impregnation. The H_2-pretreated support (0.370 g) was dispersed in an aqueous solution containing $IrCl_3{\cdot}xH_2O$ (1.37 mg, corresponding to 0.74 mg of Ir). The suspension was stirred for 12 h at room temperature. The solvent was removed via rotary evaporation, dried at 80 °C overnight, and calcined in air at 300 °C for 3 h.

Preparation of K-FexOx/CuO/ZnO/ZrO_2 Mixed Oxide Catalyst

An in situ co-precipitation approach was utilized. Precursors including $ZrO(NO_3)_2{\cdot}xH_2O$ (2.8 g), $Fe(NO_3)_3{\cdot}9H_2O$ (2.17 g), $Zn(NO_3)_2{\cdot}6H_2O$ (0.91 g), $Cu(NO_3)_2{\cdot}3H_2O$ (0.38 g), and KNO_3 (0.15 g) were dissolved in 40 mL of deionized water and stirred at 300 rpm until a clear acidic solution formed. A basic solution of Na_2CO_3 (2.0 g in 20 mL deionized water) was added dropwise until the pH reached 9. The resulting slurry was aged at room temperature for 2 h, vacuum filtered, and dried overnight. The material was calcined at 500 °C (ramp rate 2 °C/min) for 4 h.

Preparation of Promoted 10% Cu/TiO_2 and 10% Cu/CeO_2 Catalysts

For the Cu/TiO_2 system, 1.2 g of TiO_2 support was sonicated in 100 mL of deionized water. A solution of $Cu(NO_3)_2{\cdot}3H_2O$ (0.456 g in 20 mL deionized water) was injected using a syringe pump. The pH was adjusted to 9.5 with diluted ammonia, stirred for 3 h, centrifuged, dried at 80 °C, and calcined at 450 °C for 4 h. Promoter addition was achieved by re-suspending 0.8 g of the 10% Cu/TiO_2 in 10 mL of water and injecting a solution of $Fe(NO_3)_3{\cdot}9H_2O$ (0.2952 g) and KNO_3 (0.032 g). The slurry was dried at 50 °C and calcined at 400 °C (ramp rate 2 °C/min) for 4 h. An identical procedure was followed for the 10% Cu/CeO_2 catalyst, substituting TiO_2 with 1.2 g of CeO_2.

3.2 Evaluation Procedure

Structural Characterization

X-ray Diffraction (XRD): XRD analysis was conducted on the synthesized solid powders to identify the crystallographic structures, confirm support phases (e.g., CeO_2, TiO_2, MgO, In_2O_3), and evaluate the dispersion or crystallinity of the active metal phases and mixed oxides.

Catalytic Reaction Testing

The CO_2 hydrogenation performance of the synthesized catalysts was evaluated using a continuous-flow fixed-bed reactor system.

Activation: Prior to evaluation, the catalyst bed was subjected to an *in situ* thermal reduction process at 300 °C for 7 h.

Reaction Conditions: The reactor was pressurized to 50 bar. A reactant gas mixture comprising CO_2 and H_2 at a molar ratio of 1:3 was fed into the reactor at a total continuous flow rate of 20 mL/min.

Thermal Evaluation: The catalytic reaction was tested over a temperature gradient ranging from 200 °C to 280 °C to establish the temperature-dependent conversion and selectivity profiles.

Product Analysis: The effluent gas stream was directly analyzed utilizing an online Gas Chromatograph (GC). The GC was equipped with a Thermal Conductivity Detector (TCD) for the quantification of permanent gases (CO_2, H_2, CO) and a Flame Ionization Detector (FID) for

analyzing hydrocarbons and oxygenated products (such as CH_4 and ethanol).

4 Results and Discussion

X-ray diffraction (XRD) measurements were conducted to evaluate the crystallographic structure, phase composition, and active metal dispersion of the synthesized pre-reaction catalysts. The corresponding diffractograms are presented in Figure 2. The structural profiles reveal significant phase variations that are highly dependent on the chosen support architecture and synthesis methodology. The XRD of the Fe-Cu/CeO_2 catalyst confirms the bulk CeO_2 support, characterized by sharp, high-intensity diffraction peaks at 28.5°, 33.1°, 47.5°, and 56.3°, corresponding to the (111), (200), (220), and (311) crystallographic planes, respectively [12, 13]. Crucially, characteristic reflections for metallic Cu, CuO, or crystalline Fe oxide phases are completely undetected. This total absence of active metal reflections indicates that the co-precipitated copper and iron species either exist at localized concentrations well below the XRD detection threshold.[13] Similarly, the XRD for the Fe-Cu/TiO_2 system is entirely dominated by the highly crystalline phases of the anatase TiO_2 (101) at 25.3°[12, 14]. The complete absence of active Cu and Fe reflections in both single-metal oxide supported systems indicates an ultra-high degree of dispersion across the support matrices [12]. For the single-atom Ir_1/MgO–In_2O_3 catalyst, the structural profile in Figure 2 prominently displays well-defined crystalline peaks corresponding to In_2O_3 (with the dominant (222) reflection at 30.6° and (400) at 35.5°) alongside reflections for MgO [12]. Consistent with the targeted 0.2 wt% metal loading, no reflections for metallic Ir or bulk IrO_2 are observed. This confirms the successful synthesis of highly dispersed single atoms without macroscopic aggregation [16].

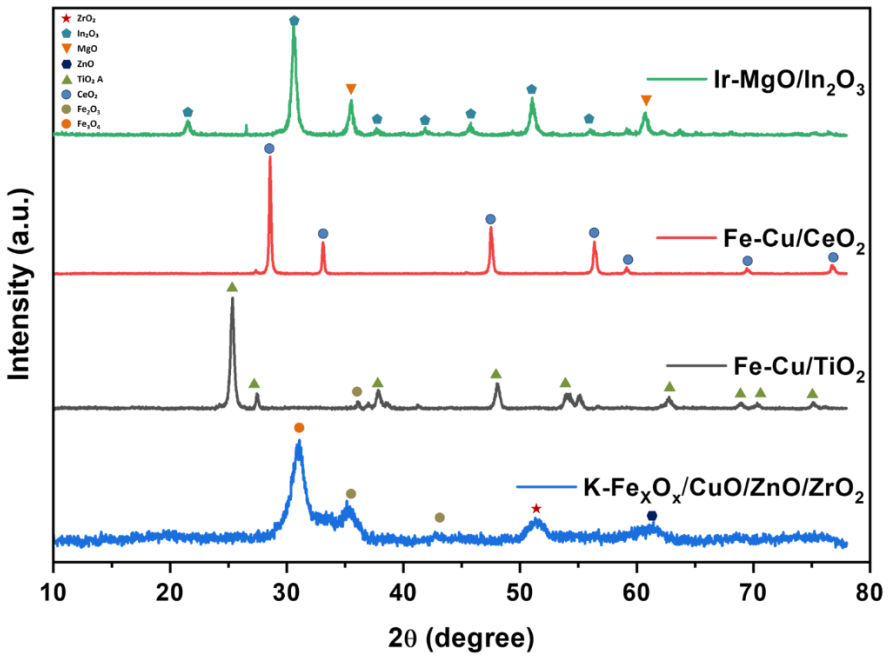


Figure 2. X-ray diffraction (XRD) patterns of the investigated pre-reaction catalysts: Fe-Cu/CeO_2, Fe-Cu/TiO_2, K-FexOx/CuO/ZnO/ZrO_2 , and Ir-MgO/In_2O_3.

In contrast, the K-promoted system (K-FexOx/CuO/ZnO/ZrO_2), synthesized via in situ co-precipitation, exhibits a highly complex mixed-oxide diffraction pattern.complex mixed-oxide diffractogram. As shown in Figure 2, the pattern reveals the formation of distinct, small crystallites of iron oxides. Specifically, characteristic reflections corresponding to Fe_3O_4 peak at 35.4° and the phase of Fe_2O_3 peak at 33.1° are readily identifiable within the matrix.[12, 15]. The relative broadening of these iron phase peaks is indicative of small average crystallite sizes, an architectural feature highly favorable for maximizing the catalytic active surface area. Additionally, weak reflections corresponding to the ZrO_2 structural phase are present. Other potential crystalline phases remain undetected, which is likely attributable to their low overall loading.

We then carried out the catalytic evaluation in the high-pressure fixed-bed reactor Figure 3 (50 bar, H_2:CO_2 ratio of 3:1) across a rigorous thermal gradient of 200 to 280 °C. Our observation revealed extreme sensitivity to these established structural architectures, exposing a profound mechanistic dichotomy governing CO_2 hydrogenation. Initial screening immediately highlighted the inefficacy of highly dispersed metals lacking contiguous active domains; the highly crystalline Fe-Cu/CeO_2 and Fe-Cu/TiO_2 supported systems exhibited negligible C_2 oxygenate synthesis activity across the entire temperature range. Despite the well-documented individual efficacies of copper for methanol synthesis and iron for the reverse water-gas shift (RWGS) reaction, their deposition on bare CeO_2 and TiO_2 supports failed to yield the necessary dual-site interfacial motifs. Consequently, the systems were unable to effectively stabilize CO* intermediates or facilitate the kinetically demanding C-C coupling steps, resulting in reaction stagnation or a strong preference for undesired C_1 byproducts.

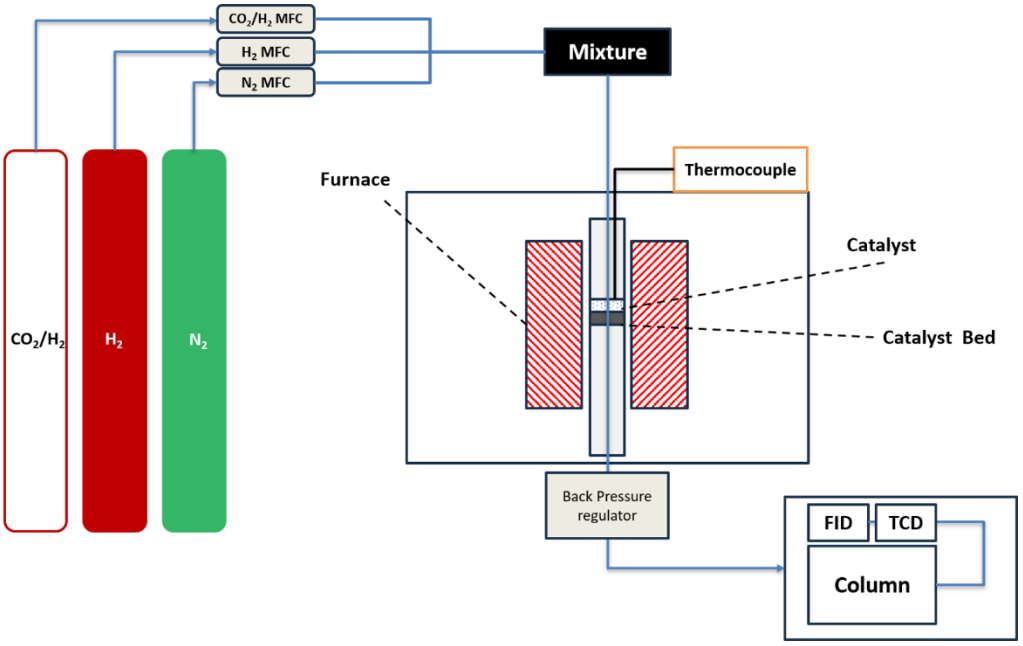


Figure 3. Schematic design of the high-pressure continuous flow reactor system utilized for the CO_2 hydrogenation evaluation.

For the functionally active catalysts, the empirical data revealed a severe "selectivity-activity trade-off" strictly dictated by thermal dynamics. For the atomically dispersed Ir/MgO–In_2O_3 catalyst, the low temperatue at 200 °C inherently restricts the initial kinetic activation of the highly stable CO_2 molecule, resulting in extremely low overall CO_2 conversion rates of less than 0.5% Figure 4a. However, despite this limited conversion, the catalyst proved uniquely effective under these

kinetically constrained conditions, achieving an exceptional ethanol selectivity of 27.5% at 200 °C Figure 4b. This high selectivity is mechanistically driven by site isolation; the lack of extended metal surfaces prevents the rapid CHx* polymerization that typically leads to broad Anderson-Schulz-Flory (ASF) hydrocarbon distributions and runaway methanation. Furthermore, operating at 200 °C thermodynamically preserves the fragile C–O bonds required for ethanol formation.

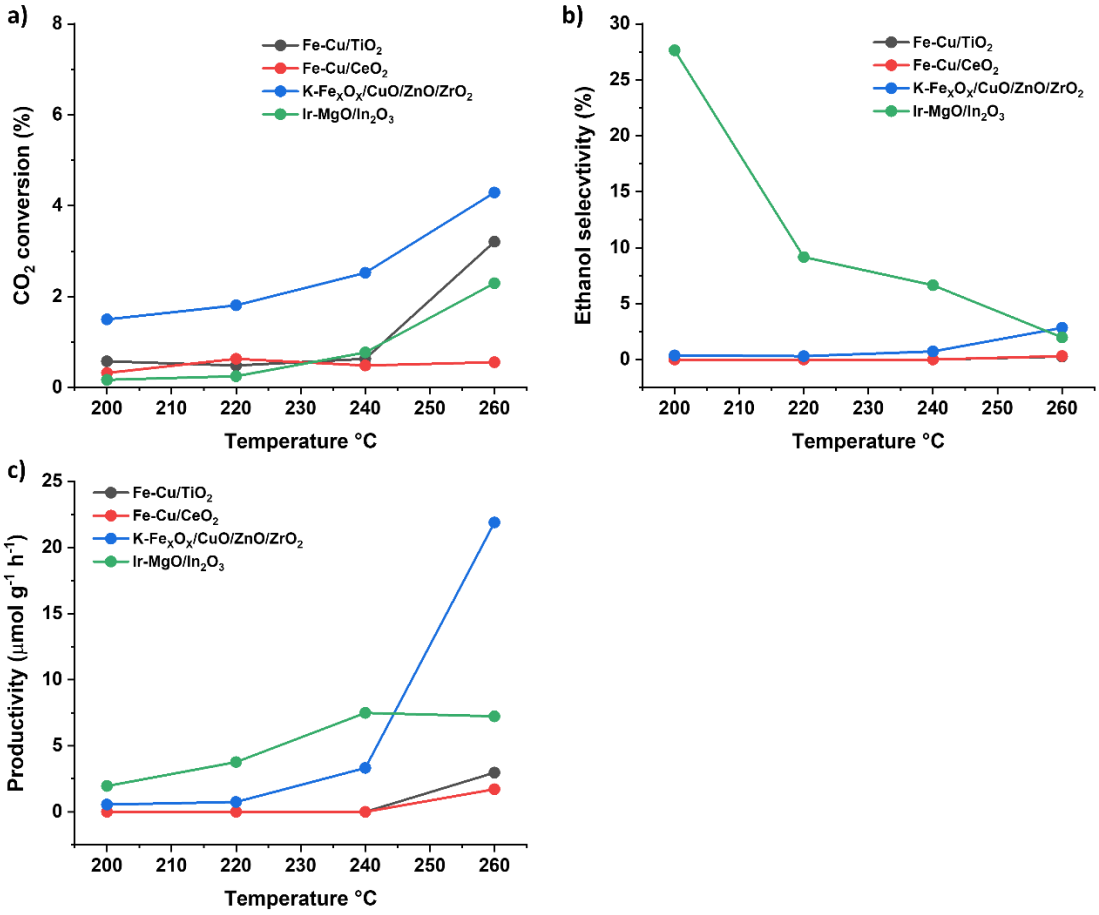


Figure 4. Temperature effects (200–260 °C) on CO_2 hydrogenation to ethanol, illustrating (a) CO_2 conversion, (b) ethanol selectivity, (c) ethanol productivity

In opposition the K-FexOx/CuO/ZnO/ZrO_2 mixed-oxide system excelled in absolute productivity at elevated temperatures, leveraging its complex multi-phase design to maximize throughput. At 260 °C, this catalyst achieved a significantly higher CO_2 conversion of 4.3%, which culminated in an optimal absolute ethanol productivity of 22 μmol g^{-1} h^{-1} figure 4c. The XRD-confirmed presence of discrete, adjacent Fe_3O_4 and Fe_2O_3 crystallite domains provides a robust tandem catalytic architecture where Fe_3O_4 efficiently drives the initial RWGS reaction to generate a high surface coverage of CO*, while the adjacent iron oxide interfaces, electronically modulated by the potassium promoter, facilitate the difficult C–C coupling sequence. However, achieving this high absolute throughput requires the elevated thermal energy of 260 °C to overcome the kinetic barrier of CO_2 activation, which introduces a severe thermodynamic penalty. The elevated temperature exponentially increases the kinetic rates of competing methanation and broad ASF chain-growth pathways, inevitably diluting the targeted C_2 oxygenate stream and explaining the sharp drop in specific ethanol selectivity to just 3%. Resolving this fundamental trade off where low temperatures are imperative for preserving C_2 selectivity via site-isolated mechanisms, while high

temperatures are requisite for driving the kinetic activation of CO_2 over mixed-oxide surfaces remains the central mechanistic challenge for advancing industrial-scale ethanol synthesis.

Table 1 Comprehensive Comparison of Synthesized Catalysts

Catalyst System	Optimal Temp (°C)	CO_2 Conv. (%)	EtOH Selectivity (%)	EtOH Productivity μmol g^{-1} h^{-1}
$Ir_1/MgO–In_2O_3$	200	0.2	27.5	2
K-FexOx/CuO/ZnO/ZrO_2	260	4.3	3.0	22.0
Fe-Cu/TiO_2	260	0.4	0	0
Fe-Cu/CeO_2	260	0.6	0	0

5 Limitations and Future Work

A significant limitation identified in this study is the inherent thermodynamic and kinetic trade-off preventing a single uniform catalyst bed from simultaneously achieving both high absolute CO_2 conversion and high targeted C_2 oxygenate selectivity. Single-metal support matrices fail to promote coupling, while highly active mixed-iron systems remain constrained by broad ASF product distributions. Future work should prioritize the design of dual-bed or tandem catalytic reactor systems. Such configurations could decouple the reaction stages, utilizing a high-temperature front bed containing a robust Fe-based catalyst to maximize initial CO_2 conversion to CO*, followed by a low-temperature secondary bed utilizing Ir-based single-atom catalysts optimized exclusively for high-selectivity C–C coupling to ethanol.

6 Conclusion

The direct thermo-catalytic conversion of CO_2 to ethanol is a vital strategy for sustainable carbon utilization but is fundamentally restricted by a severe selectivity-activity trade-off. This study demonstrates that precise active-phase engineering can selectively navigate these thermodynamic barriers. We established that an atomically dispersed $Ir_1/MgO–In_2O_3$ catalyst achieves exceptional ethanol selectivity of 27.5% at a low temperature of 200 °C by circumventing traditional extended-metal methanation pathways. In contrast, K-promoted mixed iron oxides in the K-FexOx/CuO/ZnO/ZrO_2 system utilize discrete small-crystallite phases of Fe_3O_4 and Fe_2O_3 to maximize overall productivity, yielding 22 μmol g^{-1} h^{-1} at an elevated temperature of 260 °C. Bridging the gap toward industrial viability will likely require the integration of these distinct catalytic profiles into synergistic tandem systems.

7 Acknowledgements

I would like to express my sincere gratitude to King Abdullah University of Science and Technology (KAUST) and the Center for Renewable Energy Storage and Technologies (CREST) for providing the explicit research experience and facilities that made this work possible. I extend my deepest thanks to Professor Kuo-Wei (Andy) Huang, Dr. Rajesh Belgamwar, and all the group members for their invaluable guidance, support, and help throughout the entirety of this project.

References

[1] Mac Dowell, N.; Fennell, P. S.; Shah, N.; Maitland, G. C. The Role of CO_2 Capture and

Utilization in Mitigating Climate Change. *Nat. Clim. Change* **2017**, *7* (4), 243–249.

[2] Friedlingstein, P.; O'Sullivan, M.; Jones, M. W.; Andrew, R. M.; Bakker, D. C. E.; Hauck, J.; Landschützer, P.; Le Quéré, C.; Luijkx, I. T.; Peters, G. P.; et al. Global Carbon Budget 2023. *Earth Syst. Sci. Data* **2023**, *15* (12), 5301–5369.

[3] International Energy Agency (IEA). Global Energy Review 2026: CO_2 Emissions. https://www.iea.org/reports/global-energy-review-2026/co2-emissions.

[4] Chatterjee, S.; Huang, K.-W. Unrealistic Energy and Materials Requirement for Direct Air Capture in Deep Mitigation Pathways. *Nat. Commun.* **2020**, *11*, 3287.

[5] Parsapur, R. K.; Chatterjee, S.; Huang, K.-W. The Insignificant Role of Dry Reforming of Methane in CO_2 Emission Relief. *ACS Energy Lett.* **2020**, *5* (9), 2881–2885.

[6] Hepburn, C.; Adlen, E.; Beddington, J.; Carter, E. A.; Fuss, S.; Mac Dowell, N.; Minx, J. C.; Smith, P.; Williams, C. K. The Technological and Economic Prospects for CO_2 Utilization and Removal. *Nature* **2019**, *575* (7781), 87–97.

[7] Arakawa, H.; Aresta, M.; Armor, J. N.; Barteau, M. A.; Beckman, E. J.; Bell, A. T.; Bercaw, J. E.; Creutz, C.; Dinjus, E.; Dixon, D. A.; et al. Catalysis Research of Relevance to Carbon Management: Progress, Challenges, and Opportunities. *Chem. Rev.* **2001**, *101* (4), 953–996.

[8] Koytsoumpa, E. I.; Bergins, C.; Kakaras, E. The CO_2 Economy: Review of CO_2 Capture and Reuse Technologies. *J. Supercrit. Fluids* **2018**, *132*, 3–16.

[9] Ye, R.-P.; Ding, J.; Gong, W.; Argyle, M. D.; Zhong, Q.; Wang, Y.; Russell, C. K.; Xu, Z.; Russell, A. G.; Li, Q.; et al. CO_2 Hydrogenation to High-Value Products via Heterogeneous Catalysis. *Nat. Commun.* **2019**, 10, 5698.

[10] Goryachev, A.; Pustovarenko, A.; Shterk, G.; Alhajri, N. S.; Jamal, A.; Albuali, M.; Gascon, J. A Multi-Parametric Catalyst Screening for CO_2 Hydrogenation to Ethanol. *ChemCatChem* **2021**, *13*, 3324–3332.

[11] Chen, Y.; Liu, J.; Chen, X.; Gu, S.; Wei, Y.; Wang, L.; Guan, G. Development of Multifunctional Catalysts for the Direct Hydrogenation of Carbon Dioxide to Higher Alcohols. *Molecules* **2024**, *29* (11), 2666.

[12] Wang, Y.; Jiang, X.; Cheng, K.; Kang, J.; Wang, Q. CO_2 Hydrogenation to Methanol and Dimethyl Ether over Bifunctional Catalysts. *ACS Catal.* **2021**, 11 (15), 9322–9336.

[13] Wang, N.; Chu, W.; Zhang, T.; Zhao, X. S. Synthesis, Characterization and Catalytic Performance of Cu-Based Catalysts Supported on CeO_2 for CO_2 Hydrogenation. *Chem. Eng. J.* **2015**, *270*, 51–57.

[14] Mutschler, R.; Moioli, E.; Luo, W.; Gallandat, N.; Züttel, A. CO_2 Hydrogenation Reaction over Pr-Promoted Ni/Al_2O_3 and Cu/TiO_2 Catalysts. *J. Catal.* **2018**, *366*, 139–149.

[15] Yan, H.; Zhao, M.; Li, L.; Wang, X. Active Sites of Iron-Based Catalysts for CO_2 Hydrogenation to Light Olefins. *ChemCatChem* **2023**, *15*, e202201389.

[16] Liu, L.; Liu, J.; Li, G.; Shi, X.; Yin, J.; Zheng, S.; Lo, T. W. B. Exceptional CO_2 Hydrogenation to Ethanol via Precise Single-Atom Ir Deposition on Functional P Islands. *Angew. Chem. Int. Ed.* **2025**.